

14 **Abstract**

15 A novel highly efficient and stable for many cycles catalyst (1%Co-ZSM-5(17))
16 for water oxidation was developed using the method of polycondensation for
17 stabilization of oxo/hydroxo complexes of cobalt (II, III) and nanosize Co_3O_4 in zeolite
18 channels. In a weak-alkaline medium (pH 8.0, 9.2, 10.0) in the presence of a one-
19 electron oxidant ($\text{Ru}(\text{bpy})_3^{3+}$), the catalyst provided the yield of oxygen as high as 56,
20 73 и 78 % of the stoichiometric quantity, respectively. Catalysts based on ZSM-5
21 zeolite exhibited higher catalytic activity as compared to the catalysts based on the
22 MOR, BEA, Y. Inspection of the electron states of cobalt in the Co-containing zeolite-
23 based catalysts using TPR- H_2 and UV-Vis DR techniques revealed that $\alpha\text{-Co}(\text{OH})_2$ -like
24 polynuclear clusters and hydrocomplexes stabilized in the zeolite channels were most
25 active to catalytic oxidation of water, while their transformation to Co_3O_4 -like
26 clusters/nanoparticles and Co^{2+} oxocomplexes, respectively, during thermal treatment
27 led to some decrease in the catalyst efficiency. Coarsening of Co_3O_4 -like
28 clusters/nanoparticles caused the further decrease in the system efficiency. The minimal
29 activity was observed with the catalysts containing predominantly isolated $\text{Co}^{2+}_{\text{OH}}$ ions.
30 The result obtained indicates a kind of at least polynuclear structure of the catalytically
31 active center Co_nO_x , where $n > 2$.

32

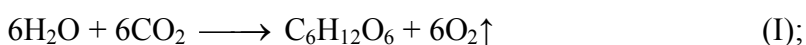
33

34 *Keywords:* water splitting, one-electron oxidants, cobalt hydroxides, zeolite,
35 oxygen evolution reaction

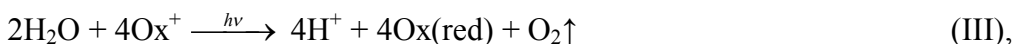
36

1. Introduction

Development of photocatalytic systems based on the transformation of solar to chemical energy is the key challenge in transition to the use of alternative energy sources with zero carbon balance [1]. In these systems, photoinitiated electron transfer from donor molecules to molecules of the electron acceptor is accompanied by the formation of energy saturated compounds such as, for example, carbohydrates in natural photosynthesis (I) or molecular hydrogen in water photodecomposition (II). Of interest are the systems with H₂O as the electron donor and CO₂ or H₂O as the electron acceptor:



The processes of carbon dioxide fixation (I) and complete water splitting (II) differ considerably but, even so, the reaction of water oxidation (III) is the limiting stages in both processes:



where Ox⁺ is a one-electron oxidant generated under the action of visible light, and Ox(red) is its reduced species. This reaction needs successive transfer of four electrons and four protons from two water molecules. However, the photocatalysts, which are excited upon absorption of unit light quantum, are only capable of generating one-electron oxidants. Therefore, a catalyst for water oxidation should be used to provide accumulation of the necessary quantity of oxidative equivalents and stabilization of intermediate products of water oxidation [2].

It is known now with certainty that some oxo/hydroxo compounds of Co(III) can catalyze water oxidation [3-8]. The efficiency of these catalysts decreases as their crystallites grow in size, and the maximal efficiency is observed with the particles less than 4 nm in diameter [9]. The reaction is conducted in weak-alkaline media where cobalt hydroxides tend to coagulate and to form bulky particles [10]. Therefore, the stabilization of highly effective nanosize particles (less than 4 nm in size) needs the presence of stabilizing ligands [11, 12]. This approach makes it possible to create colloidal systems that are appropriate for studying the reaction mechanism [7, 12]. Heterogeneous catalysts are of more practical interest. In these catalysts, the nanosize particles are stabilized using a support; the support not only prevents coarsening of the particles of Co(III) hydroxo compounds but also changes their electron structure due to

71 the interaction with the support surface. The typical supports are oxides of silicon [13]
72 or aluminium [14], oxidized carbons [15, 16, 17], nitrogen doped carbon nanotubes
73 [18], polyoxometallates [7, 19,20] and the other oxide materials [21].

74 | A wide variety of the aluminosilicate supports [22] makes them applicable for
75 stabilization of oxo/hydroxo compounds of transition metals and allows the size of
76 catalytically active species and electron state of the active component to be finely
77 adjusted. It was shown with oxides MnO_x as an example that their stabilization on the
78 zeolite support NaY [23] provided a high efficiency of the catalyst for water oxidation
79 (TOF 0.44-1.67 mmol $O_2 \cdot mol^{-1} Mn \cdot s^{-1}$). In the present work we used zeolites with
80 different topology and modulus (Si/Al ratio) for stabilization of oxo/hydroxo
81 compounds of Co (II,III). Variations in the methods for the catalyst synthesis
82 (impregnation of H-zeolite with a Co salt solution, polycondensation of the active
83 component in the zeolite channels via hydrolysis of hydrated Co(II) cations under
84 controlled conditions) the state of the active component to change considerably. From
85 literature data [24], polycondensation is an optimal method for stabilization of one-
86 dimensional nanoclusters of CoO and $CoAl_2O_4$ in channels and mesopores of H-ZSM-5
87 zeolite, while the size, localization and electron state of cobalt cations in the
88 oxo/hydroxo compounds may be controlled via intentional choice of the NH_4OH/M^{2+}
89 ratio and variations in the content of the active metal in the zeolite; that has been
90 demonstrated earlier with Cu(II) cations stabilized in H-ZSM-5 [25]. However, data on
91 the influence of the said parameters on the state of cobalt ions stabilized in the zeolite
92 matrix are unavailable in literature.

93 | Development of high-effective catalysts for water oxidation with the one-
94 electron oxidant $Ru(bpy)_3^{3+}$ based on hydroxo/oxo compounds of Co needed systematic
95 studies of the influence of synthetic parameters (morphology and modulus (Si/Al ratio)
96 of the zeolites, quantity, the NH_4OH/M^{2+} ratio and supporting procedure of the active
97 component) on the composition, structure and localization of the oxo/hydroxo
98 complexes of Co, characterization of catalytic behavior of the prepared samples, as well
99 as revealing of the correlation between physicochemical and catalytic properties of the
100 catalysts. The aim of this article is an aims at identification, elucidation of these
101 relationships.

102 |

103 2. Materials and methods

104 *Chemicals and materials*

105 The following reagents were used: Ru(OH)Cl₃ (pure), H₂SO₄ (high pure), HNO₃
106 (high pure), HClO₄ (high pure), NaOH (Panreac), NaClO₄ (high pure), Na₂HPO₄
107 (analytically pure), NaH₂PO₄ (analytically pure), CoCl₂·6H₂O (pure). All the solutions
108 were prepared with deionized water obtained using a Milli-Q (Millipore) treatment
109 system.

110 Complex Ru(bpy)₃(ClO₄)₃ as the oxidant was prepared by oxidizing
111 Ru(bpy)₃(ClO₄)₂ with PbO₂ [26]. Complex Ru(bpy)₃(ClO₄)₂ was synthesized from
112 Ru(OH)Cl₃ using the known procedure [27]. From UB-Vis data obtained at λ=452 nm
113 (ε=14 000) using Agilent Cary 60, USA, there was no more than 5 % of the initial two-
114 valent complex in the prepared oxidant.

115 *Catalyst preparation*

116 Co-ZSM-5 catalysts were prepared by polycondensation of hydrated Co(II) ion
117 in the zeolite pores [21], some of the synthetic parameters were optimized [22] in order
118 to stabilize oxo/hydroxo clusters of transition metals. The zeolite, after its incipient
119 wetness impregnation with a cobalt chloride solution, was treated with the solution of
120 ammonia at the required concentration at room temperature for 24 hours. The modified
121 samples were filtered, washed with distilled water and dried in air to obtain free flowing
122 sample, then at 120 °C for 2 hours. The resulting samples were calcined at 500 °C for 4
123 hours.

124 Five series of Co-ZSM-5 catalysts were prepared by this method. In the first
125 series, the NH₄OH/Co²⁺ (α) ratio was varied (3, 6, 10, 15, 20, 30) by varying the
126 ammonia concentration at the constant cobalt content (1 wt %). H-ZSM-5 zeolite with
127 Si/Al=17, 95 % crystallinity and no more than 0.09 wt % of Fe impurity was used for
128 the preparation. From ²⁷Al NMR data, there was no more than 10 % of extralattice Al³⁺
129 complexes [28].

130 In the second series, the cobalt content was carried (0.1, 0.5, 1 and 2 wt %) at the
131 constant NH₄OH/Co²⁺ (α) ratio equal to 6; H-ZSM-5 zeolite with Si/Al = 17 was used.

132 In the third series, the silica ratio of H-ZSM-5 (from Khimkontsentrat, Russia)
133 was varied as 17, 30 and 45 at the cobalt content equal to 1 wt % and NH₄OH/Co²⁺ ratio
134 (α) to 6. H-ZSM-5 zeolites with Si/Al = 30 and 45 comprised no more than 0.6 wt % of
135 extrinsic Fe cations [26].

136 In the fourth series, the chemical composition and structure of Y, MOR, BEA
137 zeolites were varied at the Co content of 1 wt % and $\alpha = 6$.

138 Catalysts of the fifth series was prepared for comparison; they were prepared by
139 impregnating H-ZSM-5(17) with the solutions of cobalt (II) chloride and
140 hexaammoniate of cobalt (II) chloride.

141 In the paper, the catalysts are symbolized as n%Co(α)-Z(s) where n is the cobalt
142 content (wt %); α is the $\text{NH}_4\text{OH}/\text{Co}^{2+}$ ratio; Z is the structural type of zeolite (ZSM-5,
143 Y, MOR, BEA); s is the silica ratio of zeolite (Si/Al ratio calculated on the basis of the
144 data of X-ray fluorescence analysis). The composition and textural properties of the
145 catalysts are shown in Table 1.

146 *Catalyst characterization*

147 UV-Vis DR spectra were acquired with BaSO_4 as the reflectance standard at
148 $11000\text{--}53000\text{ cm}^{-1}$ using a UV-2501 PC spectrophotometer from Shimadzu equipped
149 with a diffuse reflectance unit ISR-240 A. The spectra are plotted in the Kubelka-Munk
150 function, $F(R_\infty)$, – wave number coordinates.

151 Temperature programmed reduction of Co-ZSM-5 with hydrogen (TPR- H_2) was
152 experimentally studied using a flow setup equipped with a thermal conductivity
153 detector. A catalyst sample (100 mg of 0.25–0.50 mm fraction) was mixed with 100 mg
154 of quartz granules of the similar size. The sample was kept in flowing oxygen (30
155 cm^3/min) at $500\text{ }^\circ\text{C}$ for 30 min in order to remove adsorbed water, then cooled to room
156 temperature and kept in flowing argon (30 cm^3/min) in order to remove oxygen from
157 the catalyst pores. To record the TPR- H_2 curve, a hydrogen-argon mixture (10 vol %
158 H_2) was passed at the rate of 30 cm^3/min through the catalyst sample heated from $20\text{ }^\circ\text{C}$
159 to $800\text{ }^\circ\text{C}$ at the rate of $10\text{ }^\circ\text{C}/\text{min}$. The formed water was frozen out at $-60\text{ }^\circ\text{C}$ in a trap.
160 The hydrogen uptake was calibrated relative to the quantity of hydrogen consumed for
161 reduction of CuO at identical conditions.

162 The TPR- H_2 tests were carried out to evaluate the activation energies for
163 cobalt oxide particles reduction by hydrogen when the heating rate was varied: 5, 10,
164 and $15\text{--}15\text{ }^\circ\text{C}/\text{min}$. We calculated the activation energy (E_a) as a slope of the line plotted
165 by the equation using linearization of the dependence [29]: of

$$166 \quad 2 \ln T_m - \ln \beta = \frac{E_a}{RT_m} + C \quad ; (2 \ln T_{\max} - \ln \beta) \text{ from } 1/T_{\max} \text{ [29]; [O1]$$

167 where β is denoted the rate of temperature increase, C is a constant relevant to
168 the experimental condition, T_{\max} is the temperature maximum in the TPR- H_2 profile
169 registered at different β (5, 10, and 15 °C/min), and R is the gas constant.

170 Here, the calculated slope of the plot related to the E_a/R , where E_a was activation
171 energy.

172 *Catalyst testing for water oxidation by $Ru(bpy)_3^{3+}$*

173 Catalysts were tested for water oxidation (WO) with complex $Ru(bpy)_3(ClO_4)_3$.
174 The oxygen yield was recorded using a Clark electrode (764080 Dissolved Oxygen
175 Probe, Germany) in line with an oxygen meter (HI 2004 edge, Germany). A plastic
176 reactor mounted in a jacketed vessel and thermostated with a thermostat (TEPMEX VT-
177 8-02) was used for the experiments. A catalyst sample (50–300 mg) was immersed in 24
178 mL buffer solution (0.06 M borate buffer at pH 9.2, 10.0 or 0.06 M phosphate buffer at
179 pH 7.00); the reactor was blown through with argon until the oxygen meter showed zero
180 oxygen, then thermostated at 298 K for 15 min. After mixing and argon blowing was
181 stopped, the aqueous solution (1 mL) containing 24 mg of $Ru(bpy)_3^{3+}$ was added. The
182 reactor was plugged hermetically during 1–2 s, stirring turned on, and the oxygen yield
183 started recorded.

184 The oxygen yield was calculated by formula:

$$185 \quad Y\% = \frac{[O_2]}{0.25 \times [Ru(bpy)_3^{3+}]_0} \times 100$$

186 where $[O_2]$ is the equilibrium concentration registered by oxygen meter after the
187 reaction, $[Ru(bpy)_3^{3+}]_0$ is the initial concentration of oxidant.

188 **3. Results and discussion**

189 *Electron state of cobalt cations in $n\%Co(\alpha)$ -Z(s) depending on the synthetic* 190 *conditions*

191 UV-Vis DR spectra (Fig. 1) were acquired with the air-dry and calcined catalysts
192 prepared by polycondensation and containing 1 wt % of a transition metal. The
193 absorption fundamental edge (AFE) seen as the absorption at the UV region (>37500
194 cm^{-1}) is characteristic of H-ZSM-5 zeolite [24]. The absence of bands of H-ZSM-5 in
195 the visible region of the spectrum allows the electron state of cobalt cations in the Co-
196 ZSM-5 catalyst to be reliably interpreted. In the UV-Vis DR spectra of 1%Co(α)-ZSM-
197 5 prepared at varied NH_4OH/Co^{2+} ratio in the range of $\alpha = 3-30$, a multiplet absorption

198 band with maxima at 14300–15300–16100 cm^{-1} and a broad asymmetric band at
199 17500–19000 cm^{-1} (Fig. 1A) is observed. The band energies correspond to the d-d
200 transition of the cations with the tetrahedral ($\text{Co}^{2+}_{\text{Td}}$) and octahedral ($\text{Co}^{2+}_{\text{Oh}}$) ligand
201 surroundings [30], respectively. However, energies of d-d transitions of Co^{2+} complexes
202 with oxygen-containing and ammonia ligands differ only slightly that makes it difficult
203 to interpret the ligand nature in the coordination sphere based on the absorption bands in
204 the UV-Vis DR spectra. From literature data [26, 31, 32], two d-d transitions (${}^4\text{T}_{2\text{g}} \text{—}$
205 ${}^4\text{T}_{1\text{g}}$ and ${}^4\text{T}_{1\text{g}}(\text{P}) \text{—} {}^4\text{T}_{1\text{g}}$) at 8100 and 19000 cm^{-1} appear in the spectra of $[\text{Co}(\text{H}_2\text{O})_6]^{2+}$
206 and $[\text{Co}(\text{H}_2\text{O})_5(\text{OH})]^+$ with the octahedral ligand coordination and at 9000 and 21000
207 cm^{-1} in the spectra of $[\text{Co}(\text{NH}_3)_6]^{2+}$. Similar phenomena are characteristic of tetragonal
208 complexes of Co^{2+} : a multiplet at 16450 – 18600 – 22250 cm^{-1} (d-d transitions ${}^4\text{A}_{2\text{g}} \text{—}$
209 ${}^4\text{B}_{1\text{g}}$, ${}^4\text{T}_{1\text{g}}(\text{P}) \text{—} 4\text{E}_{\text{g}}$, ${}^4\text{T}_{1\text{g}}(\text{P}) \text{—} 4\text{A}_{2\text{g}}$) for $[\text{Co}(\text{H}_2\text{O})_4]\text{Cl}_2$ and at 16000 – 18000 – 19200
210 cm^{-1} (d-d transition $4\text{T}_1(\text{P}) \text{—} 4\text{A}_2$) for $[\text{Co}(\text{NH}_3)_4]^{2+}$ [30]. Analysis of the state of Co^{2+}
211 cations is made even more difficult due to possible interaction between the active
212 component and the support that may occur in heterogeneous systems to shift absorption
213 | bands by 1000–2000 cm^{-1} .

214 Two experimental observations should be analyzed for identification of the
215 complex compositions. First, in the spectrum of the impregnated sample 1%Co(0)-
216 ZSM-5-IWI prepared by incipient wetness impregnation of the zeolite with the CoCl_2
217 solution without further treatment with ammonia contains bands at 14300-15300-16100
218 (multiplet) and 17500-21200 cm^{-1} with maxima close in energy to those of $[\text{Co}(\text{H}_2\text{O})_4]^{2+}$
219 and $[\text{Co}(\text{H}_2\text{O})_6]^{2+}$ [28], respectively. Hence, the multiplet at 14300-15300-16100 cm^{-1}
220 relates to nanoparticles of a salt with the structure close to $[\text{Co}(\text{H}_2\text{O})_4]\text{Cl}_2$ localized in
221 the pore structure of the zeolite. A broad band at 17500-21200 cm^{-1} is assigned to
222 isolated $[\text{Co}(\text{H}_2\text{O})_6]^{2+}$ cations in the zeolite cation-exchange positions formed through
223 ion exchange with zeolite protons during the impregnation with cobalt chloride at
224 pH 3.5. Cations $[\text{Co}(\text{H}_2\text{O})_6]^{2+}$, which are characterized by the absorption band at 19500
225 cm^{-1} , were identified earlier in the spectra of hydrated Co-ZSM-5 prepared by wet ion
226 exchange with solutions of $\text{Co}(\text{NO}_3)_2$, CoCl_2 and $\text{Co}(\text{CH}_3\text{COO})_2$ [33-35].

227 Second, two weakly resolved multiplet at 14300-15300-16100 cm^{-1} and 16000-
228 17500-18500 cm^{-1} are observed in the spectrum of 1%Co(24)-ZSM-5-IWI prepared by
229 the impregnation with water-ammonia solution of $[\text{Co}(\text{NH}_3)_6]^{3+}$ with the ratio
230 $\text{NH}_4\text{OH}/\text{Co}^{2+} = 24$ (the spectrum is not presented) that results in apparent violation of
231 intensity ratios in both multiplets. The former multiplet energy (14300-15300-16100
232 cm^{-1}) relates, as discussed above, to $\text{Co}^{2+}_{\text{Td}}$ cations. Since Co^{2+} amines are easily

233 destroyed to Co(OH)_2 in water, it is reasonable to suppose that $\text{Co}^{2+}_{\text{Td}}$ cations are
234 involved in Co(OH)_2 . The latter multiplet energy corresponds almost ideally to the
235 energy of d-d transition ${}^4\text{T}_1(\text{P}) - {}^4\text{A}_2$ to $[\text{Co(NH}_3)_4]^{2+}$ (16000 – 18000 – 19200 [28]). On
236 the other hand, the said absorption bands can be assigned to ammine complexes of Co^{3+}
237 with different coordination spheres, for example: $[\text{Co(NH}_3)_5\text{Cl}]^{2+}$ (18720, 21350, 27500
238 cm^{-1} [28]), $[\text{Co(NH}_3)_4\text{Cl}]^+$ (15900, 21000, 24940 cm^{-1} [Ошибка! Закладка не
239 определена.28]) and $[\text{Co(NH}_3)_3\text{Cl}_3]$ (15800, 17500 cm^{-1} [28]). Note that multiplet
240 16000-17500-18500 cm^{-1} is observed in the spectrum of the sample dried at 120 °C but
241 absorption bands at 11000 cm^{-1} (weak), 18000 - 21000 cm^{-1} and 25000-33000 cm^{-1}
242 (intense) in the spectrum of the impregnated sample. The presence of bands with the
243 energy characteristic of $[\text{Co(NH}_3)_6]^{3+}$ (13000, 21200, 29600 cm^{-1} [28]) indicates the
244 formation of complexes $[\text{Co(NH}_3)_4]^{2+}$ and/or $[\text{Co(NH}_3)_{6-x}\text{Cl}_x]^{(3-x)+}$ from $[\text{Co(NH}_3)_6]^{3+}$ in
245 the course of drying. Thus, sample 1%Co(24)-ZSM-5-IWI there are hydroxide-like
246 nanoparticles which comprise $\text{Co}^{2+}_{\text{Td}}$ cations in the zeolite pore space and various
247 ammine complexes $[\text{Co(NH}_3)_4]^{2+}/[\text{Co(NH}_3)_{6-x}\text{Cl}_x]^{(3-x)+}$ in the cation positions of the
248 zeolite.

249 Let us compare UV-Vis DR spectra acquired with the samples prepared by
250 polycondensation and impregnation. First, in the spectra of air-dry samples prepared by
251 polycondensation in the presence of ammonia, the band at 17500 – 21200 cm^{-1} is shifted
252 towards lower wave numbers (approximately, 1000 cm^{-1}) and increases in intensity with
253 an increase in the $\text{NH}_4\text{OH}/\text{Co}^{2+}$ from 0 to 15 and then changes in non-linear manner at
254 $\text{NH}_4\text{OH}/\text{Co}^{2+} = 20$ and 30. Unlike a.b. 17500 – 21200 cm^{-1} , the triplet band energy is
255 practically independent of $\text{NH}_4\text{OH}/\text{Co}^{2+}$ in the range of 6 to 30, and the apparent change
256 in its intensity is accounted for by overlapping with the band at 17500 – 21200 cm^{-1} .
257 The said spectral features indicate the presence of $\text{Co}^{2+}_{\text{Td}}$ (14300-15300-16100 cm^{-1})
258 and $\text{Co}^{2+}_{\text{Oh}}$ (17500-21200 cm^{-1}) cations. The polycondensation includes the following
259 chemical processes occurring in micro- and mesopores of the zeolite: (1) hydrolysis of
260 $[\text{Co(H}_2\text{O)}_6]^{2+}$ cations resulting from the local changes in pH upon addition of the
261 ammonia solution; (2) polycondensation of $[\text{Co(OH)}]^+$ to $[\text{Co}_2(\text{OH})]^{3+}$, $[\text{Co}_4(\text{OH})_4]^{4+}$
262 and Co(OH)_2 [36]. Thus, $\text{Co}^{2+}_{\text{Td}}$ and $\text{Co}^{2+}_{\text{Oh}}$ cations are constituents of polynuclear
263 hydroxoclusters. As the $\text{NH}_4\text{OH}/\text{Co}^{2+}$ ratio increases, ligands $\text{H}_2\text{O(OH)}$ are substituted
264 for by NH_3 in the coordination sphere of $\text{Co}^{2+}_{\text{Oh}}$ cation that leads to gradual decrease of
265 $[\text{Co}_x(\text{OH})_y]$ -like clusters in size and, at the limit, to their complete dissolution and
266 formation of ammonia complexes $[\text{Co(NH}_3)_n]^{2+}$, the complete dissolution is observed at
267 a high ammonia concentration at $\text{NH}_4\text{OH}/\text{Co}^{2+}$ ratio no less than 18. Complexes

268 $[\text{Co}(\text{NH}_3)_n]^{2+}$ exchange with protons of the zeolite and are stabilized in its cation
269 positions. When the $\text{NH}_4\text{OH}/\text{Co}^{2+}$ ratio increases from 3 to 30, the proportion of
270 $[\text{Co}(\text{NH}_3)_n]^{2+}$ increases, d-d transition at ca. 19500 cm^{-1} and a multiplet at $16000\text{-}17500\text{-}$
271 18500 cm^{-1} being characteristic of $[\text{Co}(\text{NH}_3)_6]^{2+}$ and $[\text{Co}(\text{NH}_3)_4]^{2+}$, respectively. Thus,
272 samples of $1\%\text{Co}(\alpha)\text{-ZSM-5}$ prepared both at low ($\alpha=3$) and high ($\alpha=30$) ratio
273 $\text{NH}_4\text{OH}/\text{Co}^{2+}$ contain hydroxide-like polynuclear species and isolated $[\text{Co}(\text{NH}_3)_n]^{2+}$
274 cations. The energy of the observed triplet in the visible range of spectra of $1\%\text{Co}(\alpha)\text{-}$
275 ZSM-5 agrees with absorption bands in the spectrum of $\alpha\text{-Co}(\text{OH})_2$ with the mixed
276 coordination of Co^{2+} cations and structural formula $[(\text{Co}^{2+}_{\text{Oh}})_{1-x}[\text{Co}^{2+}_{\text{Td}}]_{2x}(\text{OH})_2]^{2x+}$ [36].
277 This spectrum contains broad bands at 16000 cm^{-1} ($\text{Co}^{2+}_{\text{Td}}$) and $17500\text{-}21000\text{ cm}^{-1}$
278 ($\text{Co}^{2+}_{\text{Oh}}$) unlike the spectra of $\alpha\text{-Co}(\text{OH})_2$ and $\beta\text{-Co}(\text{OH})_2$ with $\text{Co}^{2+}_{\text{Oh}}$ cations (triplet at
279 $19000\text{-}20000\text{-}21200\text{ cm}^{-1}$ and a broad band at $19000\text{-}21200\text{ cm}^{-1}$, respectively) [35, 38].
280 Hydroxide $\alpha\text{-Co}(\text{OH})_2$ with the mixed coordination of Co^{2+} ions is defect in respect of
281 hydroxide anion; therefore the charge of $[(\text{Co}^{2+}_{\text{Oh}})_{1-x}[\text{Co}^{2+}_{\text{Td}}]_{2x}(\text{OH})_2]^{2x+}$ is compensated
282 by anions of acid residues [35, 39, 40], e.g. Cl^- in the case under consideration. It was
283 suggested earlier that Co-ZSM-5 comprises oligomers oxohydroxide $[\text{CoOH-CoO}]^+$
284 identified with the triplet at $14500\text{-}16100\text{ cm}^{-1}$ in UV-Vis DR spectra [33], the
285 hydrolysis of $[\text{Co}(\text{H}_2\text{O})_6]^{2+}$ inside the channels followed by polycondensation
286 (oxolation/olation) at the thermal treatment being considered as the main reason for the
287 formation of the oxohydroxides. Baes et al. [31] discussed the presence of oxide-like
288 clusters CoO_x (with the so-called extralattice oxygen) in Co-ZSM-5 prepared via solid-
289 phase ion exchange; they suggested that CoO_x -like clusters comprise both $\text{Co}^{2+}_{\text{Td}}$ and
290 $\text{Co}^{3+}_{\text{Td}}$ cations. The latter are identified as the shoulder at 24000 cm^{-1} in the UV-Vis DR
291 spectrum.

292 Second, a weak absorption at $27500\text{-}32500\text{ cm}^{-1}$ is observed in UV-Vis DR
293 spectra of air-dry samples $1\%\text{Co}(\alpha)\text{-ZSM-5}$ (Fig. 1A). The band energy corresponds to
294 the d-d transition in the structures with Co^{3+} cations in octahedral surrounding ($\text{Co}^{3+}_{\text{Oh}}$)
295 of oxygen-containing (24700 cm^{-1} [30]) and/or ammonia (29550 cm^{-1} [30]) ligands, as
296 well as ligand-to-metal charge transfer band (CTB L-M) of polynuclear complexes of
297 Co^{2+} with bridging ligands [30]. In view of the fact of the symbate increase in intensity
298 of the mulriplet band at $14500\text{-}15300\text{-}16100\text{ cm}^{-1}$ ($\text{Co}^{2+}_{\text{Td}}$) with the intensity of band
299 $27500\text{-}32500\text{ cm}^{-1}$ ($\text{Co}^{3+}_{\text{Oh}}$), it is reasonable to suppose that $\text{Co}^{2+}_{\text{Td}}$ and $\text{Co}^{3+}_{\text{Oh}}$ cations
300 are comprised in the same compounds, for example polynuclear hydroxo complex of
301 cobalt (II,III) with the structure close to the defect $\alpha\text{-Co}(\text{OH})_2$. Unfortunately, it is
302 hardly possible to correlate directly the intensity of the band at 27500 cm^{-1} with the

303 content of $\text{Co}^{3+}_{\text{Oh}}$ catalytic activity of 1%Co(α)-ZSM-5 to water decomposition because
304 CTB L-M of hydroxo/oxo clusters of Co^{2+} and extralattice species with Cl^- -modified
305 Al^{3+} ions may appear at the same spectral region. We observed earlier the band at 27500
306 cm^{-1} in the spectra of Cu-ZSM-5 prepared by polycondensation [22].

307 Third, we cannot exclude that the 1%Co(30)-ZSM-5 sample prepared at a high
308 $\text{NH}_4\text{OH}/\text{Co}^{2+}$ ratio comprises isolated $[\text{Co}(\text{NH}_3)_6]^{3+}$ ions which give a low-intense band
309 at 13000 cm^{-1} , a band at 21000 cm^{-1} , and a shoulder at 30000-33000 cm^{-1} (d-d
310 transitions $^1\text{A}_g - ^1\text{T}_{1g}$ and $^1\text{A}_g - ^1\text{T}_{2g}$ [28]). In the spectrum of 1%Co(24)-ZSM-5-IWI
311 prepared by impregnation with a water-ammonia solution of $[\text{Co}(\text{NH}_3)_6]^{3+}$ (dark cherry
312 colored) at $\text{NH}_4\text{OH}/\text{Co}^{2+} = 24$ and dried at 25 °C these bands also were observed but
313 disappeared after drying at 120 °C to indicate the removal of NH_3 ligands from the
314 coordination sphere of Co^{3+} cations. This is consistent with the ability of $[\text{Co}(\text{NH}_3)_6]^{2+}$
315 to be gradually oxidized by air oxygen to $[\text{Co}(\text{NH}_3)_6]^{3+}$ [41]. EPR technique was used
316 [32] to observe the formation of $[\text{Co}^{3+}(\text{NH}_3)_{x-1}(\text{O}_2^-)]^{2+}$ adducts through interaction of
317 Co^{2+} in Co-ZSM-5 with ammonia at room temperature in oxygen-containing
318 atmosphere. Hence, $\text{Co}^{3+}_{\text{Oh}}$ cations can form via intraspheric electron transfer from Co^{2+}
319 to O_2 at the stage of polycondensation of hydrolyzed $[\text{Co}(\text{H}_2\text{O})_5(\text{OH})]^+$ ions in
320 concentrated ammonia solutions.

321 When air-dry 1%Co(α)-ZSM-5 catalysts are calcined in air at 500 °C (Fig. 1B),
322 defect $\alpha\text{-Co}(\text{OH})_2$ -like clusters are transformed to oxide-like clusters with the electron
323 structure similar to that of spinel with $\text{Co}^{2+}_{\text{Td}}$ (14400-16000 cm^{-1}) and $\text{Co}^{3+}_{\text{Oh}}$ (24500-
324 32500 cm^{-1}) cations, while isolated $\text{Co}^{2+}_{\text{Oh}}$ ions (19000-21000 cm^{-1}) are still in cation
325 positions of the zeolite. The calcined catalyst 1%Co(24)-ZSM-5-IWI was an only
326 sample containing isolated $\text{Co}^{2+}_{\text{Oh}}$ (d-d 19000 cm^{-1} , the spectrum is not presented) but
327 not Co_3O_4 -like clusters. Temperature genesis of $\alpha\text{-Co}(\text{OH})_2$ -like clusters in channels of
328 1%Co(α)-ZSM-5 is consistent with transformations characteristic of bulk hydroxide $\alpha\text{-}$
329 $\text{Co}(\text{OH})_2$. For example, thermal decomposition of $\alpha\text{-Co}(\text{OH})_2$ at 300 °C results in the
330 formation of Co_3O_4 in air and CoO in argon [42]. On the other hand, FTIR studies
331 indicate the formation of CoO from oligomers clusters $[\text{CoOH-CoO}]^+$ in the course of
332 thermal treatment of Co-ZSM-5 [33]. Literature data on changes in the oxidation degree
333 of Co^{2+} to Co^{3+} during oxidative treatment are somewhat contradictory. Some
334 researchers suggest that Co^{2+} is oxidized to Co^{3+} during thermal treatment of Co(II)-
335 containing materials [31, 37] but the others deny the oxidation of Co^{2+} to Co^{3+} at below
336 450 °C [21, 32, 33].

337 Co_3O_4 -like clusters containing $\text{Co}^{2+}_{\text{Td}}$ cations (triplet at 14400-15300-16000
338 cm^{-1}) and $\text{Co}^{3+}_{\text{Oh}}$ (24500-32500 cm^{-1}), and isolated $\text{Co}^{2+}_{\text{Oh}}$ cations (19000-21000 cm^{-1})
339 were observed in the other series of catalysts $n\%\text{Co}(6)\text{-Z}(s)$ prepared using H-ZSM-5
340 with different silicate ratios and the other type zeolites (BEA, MOR, Y), as well as with
341 different cobalt contents. UV-Vis DR studies of these catalysts revealed that an increase
342 in the silica ratio (from 17 to 45, no illustration) leads to an increase in the proportion of
343 Co_3O_4 -like clusters in the calcined catalysts $1\%\text{Co}(6)\text{-Z}(s)$ (where $s = 17, 30$ and 45),
344 the proportion of isolated $\text{Co}^{2+}_{\text{Oh}}$ ions being naturally decreased. This trend is natural
345 because the increase in the silica ratio results in a decrease in the cation exchange
346 positions in ZSM-5 zeolite, which are necessary for binding the isolated $\text{Co}^{2+}_{\text{Oh}}$ ions
347 [26]. Note that there is a trend to the formation of CoO-like species apart from Co_3O_4 -
348 like clusters in the calcined samples of $1\%\text{Co}(6)\text{-ZSM-5}(30)$ and $1\%\text{Co}(6)\text{-ZSM-5}(45)$.
349 The latter clusters give absorption bands at 13200 and 21000 cm^{-1} [30]. The maximal
350 proportion of the CoO-like clusters is characteristic of $1\%\text{Co}(6)\text{-ZSM-5}(30)$.

351 In calcined catalysts $1\%\text{Co}(6)\text{-Z-5}(s)$ prepared using zeolites with different
352 topology, the proportion of Co_3O_4 -like clusters increases in the series ZSM-5 > BEA >
353 Y >> MOR. Absorption bands at 14500-15300-16100, 18500-19900 and 27500 cm^{-1} are
354 assigned to these clusters. Note that $1\%\text{Co}(6)\text{-MOR}$ was an only catalyst where the
355 quantity of isolated Co^{2+} ions was more than that of Co_3O_4 clusters; seemingly, the ions
356 were stabilized in cation positions of the zeolite (18900 cm^{-1}). Again, this as an only
357 sample that became pink colored upon addition of ammonia solution (for
358 polycondensation of Co^{2+} ions) that may indicate stabilization of $\beta\text{-Co}(\text{OH})_2$ [43] and/or
359 isolated $\text{Co}^{2+}_{\text{Oh}}$ ions [28]. The blue-and-green color of all the other $n\%\text{Co}(\alpha)\text{Z}(s)$
360 samples, before they were calcined, is characteristic of $\alpha\text{-Co}(\text{OH})_2$ comprising $\text{Co}^{2+}_{\text{Td}}$,
361 $\text{Co}^{2+}_{\text{Oh}}$, and $\text{Co}^{3+}_{\text{Oh}}$ cations [35, 41]. Similar to above discussed $1\%\text{Co}(6)\text{-ZSM-5}$, air-
362 dry samples based on Beta and Y zeolites gave differently intense a.b. at 14400-15000-
363 15900, 16200-17500-18500 and 27500 cm^{-1} in the spectra.

364 The influence of cobalt content on its electron state in $n\%\text{Co}(6)\text{-ZSM-5}(17)$ with
365 n varied between 0.1 and 2 wt % is exemplified in Fig. 2. Inspection of the UV-Vis DR
366 spectra shows the appearance of new electron states, which differ from those in the
367 above discussed $1\%\text{Co}(6)\text{-ZSM-5}(17)$, both at lower (0.1, 0.5 wt %) and at higher (2 wt
368 %) contents of cobalt. In the UV-Vis DR spectra of air-dry samples of $0.1\%\text{Co}(6)\text{-}$
369 $\text{ZSM-5}(17)$ and $0.5\%\text{Co}(6)\text{-ZSM-5}(17)$, there are bands at 27700 and 32500 cm^{-1} that
370 are not observed in the spectrum of $1.0\%\text{Co}(6)\text{-ZSM-5}(17)$. Absorption bands at 13200,
371 19000, 27700 and 36200 cm^{-1} are characteristics of the calcined low-loaded samples.

372 **Apparently**, polycondensation of hydrolyzed cobalt ions in pores of the catalyst with the
373 low cobalt content and, respectively, low ammonia concentration results in predominant
374 formation of $[\text{Co}(\text{OH})]^+$ cations and CoOOH nanoclusters but not polynuclear species
375 similar to the 1%Co(6)-ZSM-5(17) catalyst. Cations of $[\text{Co}(\text{OH})]^+$ are transformed to
376 $[\text{Co-O-Co}]^{2+}$ structures with CTB L-M 27700 and 32500 cm^{-1} during drying and to CoO
377 during thermal treatment. However, there is a low proportion of CoO -like clusters in
378 0.5%Co(a6)-ZSM-5(17) in comparison to isolated $\text{Co}^{2+}_{\text{oh}}$ (19000 cm^{-1}) ions in the
379 exchange positions of the zeolite.

380 Along with the triplet at 14400-15000-15900 cm^{-1} and the slowly growing
381 absorption at 20000 – 33000 cm^{-1} , a triplet at 15900-17700-18700 cm^{-1} appears in the
382 spectrum of the air-dry sample 2%Co(6)-ZSM-5(17); the energy of this triplet is close
383 to ammonia complexes of Co^{3+} in various ligand surroundings [30]. Upon calcining,
384 2%Co(6)-ZSM-5(17) comprises Co_3O_4 -like clusters ($\text{Co}^{2+}_{\text{Td}}$ 13200, 14600 and 16100
385 cm^{-1} ; $\text{Co}^{3+}_{\text{oh}}$ 27700 cm^{-1}) and isolated Co^{2+} ions in exchange positions of the zeolite
386 ($\text{Co}^{2+}_{\text{oh}}$ 18500 cm^{-1}). It seems like a part of Co_3O_4 -like clusters reside in the zeolite
387 mesopores and not interact with the zeolite matrix.

388 *Redox properties of catalysts n%Co(α)-Z(s)*

389 Data on the electron state of cobalt cations in the n%Co(α)-ZSM-5 catalysts
390 were clarified using the TPR- H_2 technique. In addition, this technique provides
391 information on redox properties of the catalysts. Experimental TPR- H_2 profiles (Figs. 3
392 and 4) were obtained with the series of catalysts prepared by varying the $\text{NH}_4\text{OH}/\text{Co}^{2+}$
393 ratio and cobalt content. Three regions of the reduction of Co^{n+} cations can be identified
394 in the profiles: low temperature (below 450 °C), moderate temperature (550–700 °C)
395 and high temperature (750–800 °C). According to literature data [44-48], these
396 temperature regions in the profiles of reduction of Co-ZSM-5 relate to reduction of
397 easily reducible CoO_x -like clusters and nanosize particles, bi- and polynuclear
398 oxocomplexes of Co^{n+} , and hard reducible Co^{2+} cations in the cation-exchange positions
399 of the zeolite, respectively. Inspection of the TPR- H_2 profiles of the n%Co(α)-ZSM-5
400 catalysts revealed that the temperature ranges of the catalyst reduction depend on the
401 $\text{NH}_4\text{OH}/\text{Co}^{2+}$ ratio during the catalyst preparation. First, temperature ranges of the
402 reduction of isolated Co^{2+} ions in the impregnated sample 1%Co(0)-ZSM-5 are identical
403 to the data on the reduction of ion-exchanges zeolites Co-ZSM-5 [43, 44], Co-MOR
404 [43, 47] (ca. 750–780 °C). However, the high-temperature peak of hydrogen uptake
405 shifts towards lower temperature for the samples at the $\text{NH}_4\text{OH}/\text{Co}^{2+}$ ratio between 3 to

406 15 as compared to the data on the reference sample 1%Co(0)-ZSM-5, i.e. from 750–780
407 °C to 650–660 °C (Fig. 3). Lowering of the temperature of reduction of Co^{nt} ions
408 indicates the presence of at least two Co^{2+} ions bound through bridging oxygen, e.g.
409 oxocomplexes of Co^{2+} , in the structures formed at the stage of polycondensation of
410 hydrolyzed Co^{2+} ions followed by calcination [43, 47]. We observed similar effects
411 before in experimental TPR- H_2 studies of Cu-substituted ZSM-5 zeolites with high Cu
412 contents obtained by impregnation with ammonia complexes of copper [50]. Second, the
413 medium temperature peak of hydrogen uptake decreases in intensity when high
414 concentrations of ammonia are used for the catalyst preparation (for example,
415 $\text{NH}_4\text{OH}/\text{Co}^{2+} = 20$ and 30), whereas a total of hydrogen consumption taken relative to
416 the quantity of supported Co^{nt} (H_2/Co) tends to grow. At $\text{H}_2/\text{Co}=0.30\text{--}0.33$, the medium
417 temperature signal in the profiles of n%Co(α)-ZSM-5 (at $\text{NH}_4\text{OH}/\text{Co}^{2+}$ between 6 and
418 15) corresponds to the reduction of 55–65 % of all the cobalt ions reduced in the
419 catalyst. The proportion of moderately reducible ions decreases down to 10–15 % in the
420 catalysts prepared at $\text{NH}_4\text{OH}/\text{Co}^{2+}$ equal to 20 and 30, while H_2/Co is practically
421 doubled (up to 0.55) in 1%Co(30)-ZSM-5. The reason is a decrease in the proportion of
422 oxoclusters of Co^{2+} , as well as a variation in their reducibility. The decrease in the
423 reducibility can be accounted for by the interaction between a part of ammine
424 complexes of $\text{Co}^{2+}/\text{Co}^{3+}$ and terminal SiOH groups at the outer zeolite surface in
425 strongly alkaline solutions to decrease in the cobalt quantity in the zeolite channels. On
426 the other hand, Ulla et al. [43] suggest that isolated Co^{2+} ions in Co-ZSM-5 are reduced
427 slowly, so that they have no time for complete reducing during the TPR- H_2 experiment.
428 Third, the width and asymmetry of the low-temperature peak of hydrogen uptake (200–
429 400 °C) indicates the non-uniform composition and localization of CoO_x -like species on
430 the surface and pores of the n%Co(α)-ZSM-5. For example, catalyst 1%Co(0)-ZSM-5
431 consumes hydrogen at rather narrow temperature range (300–380 °C) but with two
432 maxima at 310 (shoulder) and 340 °C. The mode of the catalyst reduction may indicate
433 the presence of Co_3O_4 in its composition. There are usually two poorly resolved peaks
434 at 325–330 and 360–430 °C in the profile of reduction of bulky Co_3O_4 particles, which
435 relate to the two-stage reduction of Co_3O_4 to CoO and then to cobalt metal [51, 52].
436 Dispersion of the Co_3O_4 particles through the surface of inert supports is accompanied
437 by drop of the reduction temperature down by 30–40 °C in the case of Co-ZSM-5 [43,
438 44]. In the profiles of 1%Co(3)-ZSM-5 and 1%Co(30)-ZSM-5 catalysts, the range of
439 hydrogen uptake is broadened as 180–420 °C; the peaks with maxima at 250–265, 310,
440 340 °C and a shoulder at 430 °C can be identified there. The first three peaks may

441 indicate the reduction of Co_3O_4 -like nanoparticles differing in size and/or the manner of
442 interaction with the support. The peak at 430 °C may relate to the reduction of CoO-
443 clusters decorated by the support [43, 48]. On the other hand, it is reported in literature
444 [53, 54] that at low temperatures (215–230 °C) bulky CoOOH is reduced to Co_3O_4 to be
445 then reduced to CoO (260–279 °C) and Co (350 °C) [53]. We cannot exclude the
446 presence of CoOOH in 1%Co(30)-ZSM-5. However, 1%Co(3)-ZSM-5 seem to contain
447 polydisperse Co_3O_4 -like nanoparticles. The proportion of polynuclear clusters is
448 maximal in 1%Co(3)-ZSM-5 and decorated particles in 1%Co(20)-ZSM-5 and
449 1%Co(30)-ZSM-5. Co_3O_4 -like clusters and isolated Co^{2+} ions are in comparable
450 quantities in 1%Co(α)-ZSM-5 catalysts prepared at $\text{NH}_4\text{OH}/\text{Co}^{2+}$ equal to 6–15, their
451 proportions being practically unchanged upon an increase in the cobalt content from 1
452 to 2 wt % (Fig. 4).

453 Note that the molar ratio of the quantity of absorbed hydrogen to the cobalt
454 content (H_2/Co) in both series catalysts n%Co(α)-ZSM-5 was much lower of the
455 stoichiometric quantity of hydrogen required for the reduction of CoO, Co_3O_4 , and
456 isolated Co^{2+} ions to the cobalt metal ($\text{H}_2/\text{Co}=1, 1.33, 1$; see Figs. 3b and 4b). This is an
457 evidence of the incomplete reduction of cobalt cations in catalysts n%Co(α)-ZSM-5.
458 The maximal H_2/Co ratio (0.55–0.6, Fig. 3b) was characteristic of the catalysts prepared
459 at the ratio $\text{NH}_4\text{OH}/\text{Co}^{2+}$ equal to 6–15. Co-containing species were most hardly
460 reduced in 1%Co(0)-ZSM-5 during TPR- H_2 experiments due to modifying the catalyst
461 surface and/or CoO_x -like species with chloride ions which usually inhibit the reduction
462 of oxides and oxide clusters of transition and noble metals [22, 48].

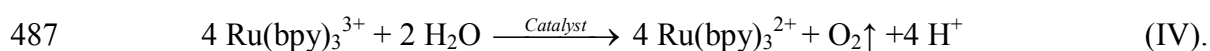
463 The shift of the hydrogen consumption peak towards higher temperatures in
464 TPR- H_2 experiments is usually caused by strong metal-support interactions [54, 55].
465 Obviously, the stronger interaction between Co_3O_4 -like particles and zeolite support, the
466 higher is the activation energy of its reduction. The observed activation energies for
467 the reduction of Co_3O_4 -like clusters or nanoparticles to CoO and the following
468 reduction of CoO to Co are shown in Table 2 for some catalysts supported on H-ZSM-
469 5(17). The minimal activation energy for the reduction of Co_3O_4 -like clusters or
470 nanoparticles was observed in the case of catalyst 2% Co(6)ZSM-5(17) ($E_a=21 \pm 3$
471 kJ/mol). It indicates that the interaction between Co_3O_4 -like clusters or nanoparticles
472 and zeolite surface is weaker than that in catalysts 1% Co(α)ZSM-5(17) with $\alpha=3-10$.

473 Thus, catalysts 1%Co(α)-ZSM-5 feature different reductability due to
474 stabilization of different electron states of Co^{n+} constituents. Isolated Co^{2+} ions in
475 cation-exchange positions of the zeolite are most stable to reduction and, most likely, do

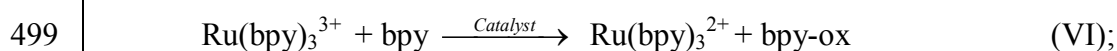
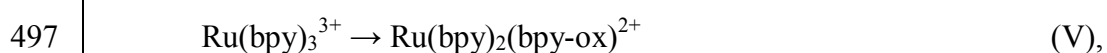
476 not participate in redox stages of water decomposition. Polynuclear oxo-species of Co^{2+}
477 were somewhat more reducible, and the highest reducibility was characteristic of
478 Co_3O_4 -like species involved in two-stage reduction: $\text{Co}^{3+} - \text{Co}^{2+} - \text{Co}^0$ that can be
479 important for stabilization of intermediate oxidation state of cobalt during water
480 decomposition.

481 *The influence of the structure type of zeolite and silica ratio on the catalytic*
482 *performance during water oxidation with complex $\text{Ru}(\text{bpy})_3^{3+}$*

483 A series of Co-containing catalysts 1%Co(6)-Z(s) based on zeolites with
484 different structures (Mordenite - MOR, Beta - BEA, Faujasite - Y, ZSM-5 - MFI) were
485 tested for the reaction (IV) of water oxidation using complex $\text{Ru}(\text{bpy})_3^{3+}$:



488
489 Note that the characteristic time of the reaction of releasing molecular oxygen
490 from water is less than 1 ms [56] but the response time of the Clark electrode used as an
491 oxygen meter ca. 30 s. When so, the data on the catalytic activity can only be obtained
492 based on the yield of oxygen. That the oxygen yields differ from 100 % of the reaction
493 IV stoichiometry is accounted for by side reactions proceeding by non-catalytic (or
494 autocatalytic) (V) and catalytic (VI) pathways of the oxidant consumption [**Ошибка!**
495 **Закладка не определена.12**]:



500
501 where bpy-ox is the oxidized bipyridyl ligand. Stage (V) of autocatalytic destruction of
502 the oxidant is responsible for a decrease in the oxygen yield at low concentrations of the
503 catalyst [57], and catalytic stage (VI) for a decrease in the oxygen yield at the high
504 concentrations of the catalyst.

505 The yields of oxygen obtained in the presence of catalysts 1%Co(6)-Z(s) are
506 shown in Table 3 (samples Nos. 1–4). Under identical conditions, the maximal yield of
507 oxygen (64 % of the stoichiometry of reaction (IV)) was observed with the catalyst
508 supported on ZSM-5 zeolite. The catalysts based on Beta and Y zeolites were similarly

509 effective and provided 60 % of the oxygen yields. The minimal oxygen yield (52 %)
510 was in the presence of 1%Co(6)-MOR(6).

511 Apparently, the different activities of 1%Co(6)-Z(s) catalysts are caused by
512 specific textures and microstructures of the zeolite, as well as by the composition of
513 catalytically active cobalt species. It was discussed above that the active components of
514 all the 1%Co(6)-Z(s) catalysts comprise (in different proportions) Co₃O₄-like
515 clusters/nanoparticles, polynuclear oxocomplexes of Co²⁺_{Oh} and isolated Co²⁺_{Oh} cations
516 in the exchange positions of the zeolite. However, the oxygen yields observed with
517 these catalysts correlated only slightly with the H₂/Co ratio in low- and high-
518 temperature regions (310–340 and >700 °C, respectively) during TPR-H₂ studies. These
519 are the regions where Co₃O₄-like clusters/nanoparticles and isolated Co²⁺_{Oh} cations,
520 respectively, are reduced. While the participation of isolated Co²⁺_{Oh} ions in water
521 oxidation is low probable due to their high stability to reduction, the catalytic behavior
522 of nanosize Co₃O₄ constituents of supported [6, 7, 11, 12, 18, 61] and colloidal [53]
523 catalysts is the subject of active discussions in literature. With our catalysts, an increase
524 in the oxygen yield in reaction IV was only observed with an increase in the proportion
525 of polynuclear oxocomplexes of Co²⁺ that were reduced at 640–660 °C during TPR-H₂
526 studies.

527 On the other hand, the observed oxygen yields depended nonlinearly on the
528 zeolite texture and on exposure of zeolite channels for stabilization of CoO_x-like
529 clusters and polynuclear particles, as well as on the chemical composition of the zeolite
530 matrix. A trend to an increase in the oxygen yield (reaction IV) was observed with an
531 increase in silica ratio in the series: ZSM-5 > Beta, Y > MOR. The increase in the
532 silicate module results in a decrease in the number of proton centers in the zeolite and,
533 correspondingly, in minimization of the site appropriate for stabilization of isolated
534 Co²⁺ ions which are inactive to the reaction under study.

535 Inspection of the correlations between zeolite channel structures and the oxygen
536 yields leads to conclude about close (64 %) or identical (60 %) selectivities of zeolite
537 catalysts with close sizes of three-dimensional channels: 5.3 × 5.6 Å and 5.1 × 5.5 Å in
538 ZSM-5; 7.6 × 6.6 Å in Beta; 7.4 × 7.4 Å in Y [59]. At the same time, complex oxidant
539 Ru(bpy)₃³⁺ is too large in size to penetrate inside these zeolite channels [7, 60].
540 Therefore, the reaction of one-electron transfer from the oxidant to the catalyst is
541 thought to occur at the channel inlet; as a result, the size and interaction of Co₃O₄-like
542 clusters with the zeolite surface and of polynuclear oxocomplexes of Co²⁺_{Oh} with
543 functional groups of the zeolite becomes of importance. Apparently, when the Co

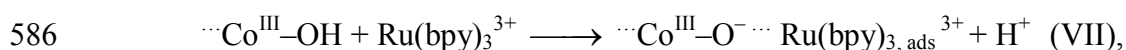
544 content is less than 1 wt %, Co_3O_4 -like clusters are formed in the zeolite channels, and
545 the channel size limits the cluster size. This assumption is supported by the similarity of
546 textural parameters such as micropore volume and external surface of the crystallites in
547 pure zeolites (ZSM-5(17) [21, 22]) and catalysts with the supported active Co-
548 component (Table 1). A topic for earlier discussions in literature was the activity of 1–2
549 nm $\text{Co}(\text{OH})_2$ particles supported on nanosize SiO_2 [61] and 3–7 nm Co_3O_4 particles on
550 silica [7]. However, these were the cases when active Co species were much larger in
551 size than the zeolite channels (no more than 0.75 nm). A decrease in the size of CoO_x
552 particles results in strengthening of their interaction with the support surface and,
553 correspondingly, in a decrease in their redox potential [62]. At the same time, a decrease
554 of the CoO_x particles in size produces more defects that is accompanied by narrowing of
555 the band gap [63] and, as a consequence, by lowering of the energy of electron transfer
556 to/from the valence band and by the trend to stabilization of higher valent Co^{III} cations.
557 It is evident that these two factors have opposite effects on the behavior of the catalytic
558 system. Therefore, in choosing the size of CoO_x particles, one should find balance
559 between the positive influence on the catalytic activity caused by the higher defectness
560 of the particles and the negative effect resulted from the lowering of the redox potential
561 of CoO_x [64].

562 On the other hand, the external surfaces of the crystallites in 1%Co(6)-beta and
563 1%Co(6)-Y were 4–6 times as large as those in 1%Co(6)-ZSM-5 (Table 1). As a result,
564 they sorb more $\text{Ru}(\text{bpy})_3^{3+}$ to accelerate side reactions V and VI and to decrease the
565 oxygen yield by reaction IV. Previously, the difference in the catalytic behavior during
566 photoinitiated water decomposition in the presence of $\text{Ru}(\text{bpy})_3^{3+}$ and persulfate was
567 accounted for by adsorption of the ruthenium complex on the larger surface of Co-
568 catalysts with nanosize Co_3O_4 particles (4 nm) supported on SBA-15 and MCM-41 [7].

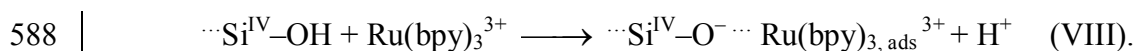
569 A series of catalysts 1%Co(6)-ZSM-5(s) prepared by polycondensation on H-
570 ZSM-5 zeolite with silica ratios 17, 30 and 45 were used for studying the influence of
571 silica ratio on the catalytic activity. The oxygen yields by the reaction of water
572 oxidation over 1%Co(6)-ZSM-5(s) are shown in Table 1, Nos. 4–6. Close oxygen yields
573 (ca. 63–64 % of the reaction stoichiometry) were observed with the zeolite with silica
574 ratio 17 and 30 but decreased down to 59 % as the Si/Al ratio was increased up to 45.
575 Apparently, an increase in the proportion of lattice Al^{3+} cations leads to an increase in
576 the concentration of proton centers in the zeolite. However, these centers reside in the
577 zeolite channels and cannot participate in the ion-exchange adsorption of the oxidant but
578 only affect indirectly the equilibrium of the ion exchange reaction with the functional

579 groups of the zeolite catalyst. The points of zero charge (pH) of H-ZSM-5(45) and H-
580 ZSM-5(17) zeolites in water are 3.4 and 3.1, respectively. Therefore, at pH 9.2 used for
581 studying the reaction of water oxidation, terminal SiOH groups of the zeolite are
582 deprotonated and can take part in the adsorption of $\text{Ru}(\text{bpy})_3^{3+}$ (VIII) the way similar to
583 the **suggested** stage of ion-exchange adsorption of the oxidant on the active site of the
584 Co-catalyst (VII) [2]:

585



587



589

590 The sorbability with respect to $\text{Ru}(\text{bpy})_3^{3+}$ increased with a decrease in the silica ratio
591 of H-ZSM-5(s) zeolites even at close external surfaces of the crystallites. The
592 sorbabilities of H-ZSM-5(17) and H-ZSM-5(45) zeolites were only 15 % different; they
593 were 8.3 and 7 mg/g, respectively (Table **3**). The difference may cause acceleration of
594 reaction IV of water oxidation but, at the same time, acceleration of side reaction VI,
595 too.

596 Of course, the proportion of Co_3O_4 -like clusters and Co^{2+} oxocomplexes is
597 higher in the zeolites with higher silica ratio (30, 45) than in the zeolites with lower
598 Si/Al (17). But apparently, the influence of the electron state of Co-constituent of
599 catalysts 1%Co(6)-ZSM-5(s) on the process efficiency was less critical under the
600 chosen reaction conditions than the influence of acid properties of the zeolite.

601 *The influence of the Co supporting procedure on the catalytic efficiency*

602 The role of the method for catalyst preparation in the formation of electron states
603 of cobalt and their catalytic activities was studied using two procedures for supporting
604 the active component on H-ZSM-5(17) zeolite: polycondensation and incipient wetness
605 impregnation. The impregnating solutions were prepared using aqueous ($\alpha=0$) and
606 water-ammonia ($\alpha=24$) solutions of cobalt chloride, the composition of the solutions
607 being identical or close to two boundary compositions used for polycondensation. The
608 first stage of the catalyst preparation via polycondensation is introduction of cobalt
609 cations into zeolite channels by impregnating the zeolite with an aqueous solution of
610 cobalt chloride. The second stage is addition of an ammonia solution of Co^{2+} cations to
611 achieve polycondensation in the zeolite channels. During the second stage, the
612 polycondensation proceeds concurrently with the complex formation to form ammonia

613 complexes of $\text{Co}^{2+}/\text{Co}^{3+}$ at the probability increasing with high α . The results of the
614 catalyst testing for water oxidation are summarized in Table 4. The tabulated data
615 demonstrate that both impregnated samples are less effective catalysts than the sample
616 prepared by polycondensation which provided the oxygen yield as high as 64 %. The
617 oxygen yields over the impregnated samples prepared with the aqueous and water-
618 ammonia solutions were 49 and 28 %, respectively. In catalyst 1%Co(6)-ZSM-5(17),
619 the active component resides in the zeolite channels in the forms of $\alpha\text{-Co}_3\text{O}_4$ -like
620 clusters, oxocomplexes of $\text{Co}^{2+}_{\text{oh}}$ and isolated $\text{Co}^{2+}_{\text{oh}}$ ions. After calcination, the
621 impregnated sample 0.5%Co(24)-ZSM-5(17)-IWI prepared with the water-ammonia
622 solution contained 0.5 wt % Co as isolated $\text{Co}^{2+}_{\text{oh}}$ in the cation-exchange positions. The
623 predomination of electron state Co^{2+} in 0.5%Co(24)-ZSM-5(17)-IWI indicates
624 unambiguously the low activity catalyst activity of the isolated $\text{Co}^{2+}_{\text{oh}}$ ions to water
625 oxidation and may bear responsibility for the low efficiency of this catalyst.

626 The predominant formation of $\alpha\text{-Co}_3\text{O}_4$ -like clusters/nanoparticles on the
627 support mesopore surface and isolated $\text{Co}^{2+}_{\text{oh}}$ in the cation positions of the zeolite was
628 observed during calcination of the impregnated sample 1%Co(0)-ZSM-5(17)-IWI
629 prepared from the aqueous solution of cobalt chloride. The suggested composition of
630 the active component of 1%Co(0)-ZSM-5(17)-IWI indicates the less efficiency of
631 Co_3O_4 -like clusters/nanoparticles for water oxidation. Again, it is not improbable that
632 the catalyst efficiency decreases due to modifying the zeolite surface and/or Co_3O_4 -like
633 clusters by chloride ions that deteriorates the reducibility of the catalyst. This
634 assumption agrees with the TPR- H_2 data on the minimal H_2/Co ratio in 1%Co(0)-ZSM-
635 5(17)-IWI among the catalysts under study.

636 *The influence of the conditions of Co-catalyst preparation on the catalytic*
637 *efficiency*

638 As shown above, the electron state and localization of the active component in
639 the zeolite can be intentionally changed by varying some conditions (quantity of
640 supported Co, $\text{NH}_4\text{OH}/\text{Co}^{2+}$ ratio, calcination temperature) of polycondensation of Co^{2+}
641 ions in zeolite pores.

642 A series of n%Co(6)-ZSM-5(17) catalysts prepared of H-ZSM-5(17) zeolite at
643 identical $\text{NH}_4\text{OH}/\text{Co}^{2+}=6$ were used for studying the influence of Co content (varied
644 between 0.1 and 2 wt %) on the efficiency of water decomposition. The oxygen yields
645 over these catalysts are shown in Table 5 (samples Nos. 1–4).

646 Note that the initial zeolite H-ZSM-5(17) was not effective, it provided less than
647 3 % yield of the stoichiometric quantity (Table 5, No. 13). Even minor quantity of
648 cobalt (0.1 wt %) supported on zeolite resulted in acceleration of the oxygen formation
649 and an increase in the oxygen yield up to 33 %. An increase in the cobalt content (up to
650 0.5 and 1.0 wt %) in n%Co(6)-ZSM-5(17) favored progressive increase in its catalytic
651 efficiency to give 55 and 64 % oxygen yields, respectively. When the cobalt content
652 reached 2 wt %, the oxygen yield decreased down to 57 %. Thus, the maximal catalyst
653 selectivity to water oxidation was observed when the Co content was no more than 1.0
654 wt %.

655 It is thought that the inefficiency of catalysts with low cobalt content (0.1 wt %)
656 results from the formation of isolated Co^{2+} ions in cation-exchange positions of the
657 zeolite. They reside preferably in the zeolite channels that make them hardly accessible
658 for $\text{Ru}(\text{bpy})_3^{3+}$, and the low efficiency is characteristics of the one-electron transfer from
659 $\text{Ru}(\text{bpy})_3^{3+}$ to the isolated Co^{2+} ions. Even though the formation of $\alpha\text{-Co}(\text{OH})_2$ -like
660 clusters and Co_3O_4 -like nanoparticles is detected in UV-Vis DR spectra of 2%Co(6)-
661 ZSM-5(17) before and after calcination, respectively, they all are localized in the zeolite
662 mesopores that results in a small decrease in the catalyst efficiency. This catalyst is
663 inferior to 1%Co(6)-ZSM-5(17) in efficiency of oxygen evolution from water. The
664 formed Co_3O_4 -like clusters degrade upon acidifying of the reaction medium during the
665 reaction, probably, because these clusters are weakly bound with the mesopore surface,
666 as TPR- H_2 data showed (Table 2). The textural characteristics of the 2%Co(6)-ZSM-
667 5(17) catalyst indicates on localization of Co_3O_4 -like clusters on the surface of the
668 mesopores, in particular the increase in outer sphere of the crystallites and the volume
669 of the mesopores (Table 1) compared to 1%Co(6)-ZSM-5(17) and pure zeolite.

670 The studies of catalytic properties of a series of 1%Co(α)-ZSM-5(17) catalysts
671 with identical contents of cobalt supported at varying the NH_4OH concentration
672 revealed that the catalyst efficiency to water decomposition depends on the
673 $\text{NH}_4\text{OH}/\text{Co}^{2+}$ ratio. The maximal yields of oxygen (63–64 %) were observed at α
674 ranging from 3 to 10. From UV-Vis DR and TPR- H_2 data, the active components of
675 these catalysts comprise predominantly Co_3O_4 -like clusters and oxocomplexes of Co^{2+} .
676 The lowest oxygen yield (50 %) was observed over the 1%Co(0)-ZSM-5(17) catalyst
677 (Table 4, No. 3) prepared similarly to the impregnated 1%Co(0)-ZSM-5(17)-IWI
678 catalyst and bearing the active component of similar composition. It is reasonable to
679 suppose that the active cobalt states are formed during polycondensation in the zeolite
680 channels through transformation of isolated and associated aquacomplexes of $\text{Co}^{2+}_{\text{OH}}$

681 and $\text{Co}^{2+}_{\text{Td}}$ to $[\alpha\text{-Co}^{2+}(\text{Co}^{3+})(\text{OH})_x]$ -like clusters and hydroxocomplexes of Co^{2+} . As α
682 increases up to 15, 20 and 30, the catalytic efficiency of oxygen evolution decreases.
683 The oxygen yields over the said catalysts were 60, 58 and 54 %, respectively. A
684 possible reason is the decrease of $[\alpha\text{-Co}^{2+}(\text{Co}^{3+})(\text{OH})_x]$ -like clusters in size and an
685 increase in the proportion of ammonia complexes $[\text{Co}(\text{NH}_3)_n]^{2+}$ in the course of
686 polycondensation.

687 Another important parameter of the catalyst preparation affecting the catalytic
688 efficiency is the temperature of sample calcination. Table 5 shows oxygen yields over
689 1%Co(3)-ZSM-5(17) and 1%Co(6)-ZSM-5(17) dried at 298 K (Nos. 11 and 12).
690 Comparison of the catalyst efficiency of the samples calcined at different temperatures
691 reveals that the calcination temperature equal to 298 and 723 K had practically no
692 influence on the catalytic properties of 1%Co(3)-ZSM-5(17). The oxygen yields were
693 63 and 64 %, respectively. However, the oxygen yields over 1%Co(6)-ZSM-5(17)
694 decreased (from 67 to 64 %) upon thermal treatment of the catalyst. Apparently, the
695 transformation of $\alpha\text{-Co}(\text{OH})_2$ -like clusters to oxide-like clusters with the structure close
696 to Co_3O_4 resulted in lowering the activity.

697 The data on the influence of parameters of preparation of $n\%\text{Co}(\alpha)\text{-Z(s)}$
698 catalysts on the composition of the active component and activity to water oxidation
699 lead to conclude that the factors determining the catalytic efficiency are both state of
700 Co^{n+} cations and the size of the formed structures/complexes, as well as textural,
701 microstructural and acid properties of the zeolite. However, the textural and
702 microstructural features do not always promote catalytic properties of the $n\%\text{Co}(\alpha)\text{-Z(s)}$
703 system. The optimal composition was characteristic of the 1%Co(6)-ZSM-5(17)
704 catalyst. Apparently, its functional groups on the zeolite surface localized on
705 comparatively small external surface of the crystallites bear responsibility for adsorption
706 of $\text{Ru}(\text{bpy})_3^{3+}$, while Co_3O_4 -like clusters and nanoparticles and oxocomplexes of Co^{2+}
707 localized in the zeolite channels close to the surface are involved in electron and proton
708 transfer.

709 *The influence of the conditions of water oxidation by $\text{Ru}(\text{bpy})_3^{3+}$ on the oxygen*
710 *yield*

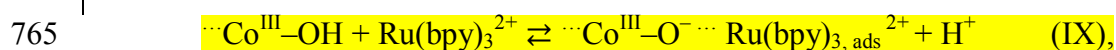
711 The most effective catalyst 1%Co(6)-ZSM-5(17) prepared by polycondensation
712 was used as an example for studying the influence of pH (7.0; 9.2; 10.0), buffer nature
713 (0.06 M borate and phosphate buffers) and catalyst concentration (10^{-4} – 10^{-3} M
714 expressed as the quantity of the active components) on the yield of oxygen (Fig. 5). The

715 curves of oxygen yield vs catalyst concentration pass through maxima that indicate
716 occurrence of processes (V) and (VI) at low and high catalyst concentrations,
717 respectively. We observed the similar behavior with colloidal Co, Fe, Mn- hydroxides
718 stabilized with starch [65]. However, in the case of colloid catalysts, the dependence of
719 the oxygen yields on the concentration of the active component was significantly lower
720 – even tenfold deviation from the optimum catalyst concentration did not significantly
721 change the oxygen yields in contrast with zeolite supported catalysts. Nevertheless, we
722 assume that the observed similarities indicate identical mechanism of the process in
723 both cases. The suggested mechanism discussed in details elsewhere [Ошибка!
724 Закладка не определена.2, Ошибка! Закладка не определена.+2]. With the
725 catalyst containing 1.1×10^{-3} M of cobalt, the maximal oxygen yields were 56, 73 and
726 78 % at pH 8.0, 9.2 and 10.0, respectively. These data are comparable to the maximal
727 oxygen yields observed in the presence of polyoxometallate complex
728 $[\text{Co}_4(\text{H}_2\text{O})_2(\text{PW}_9\text{O}_{34})_2]^{10-}$ (64% at pH 8) [66], colloidal starch stabilized cobalt
729 hydroxide (54, 73, 82% and pH 7.9, 9.2 and 11.0, respectively) [12] but inferior to the
730 yields over Co(II) hydroxide stabilized on silica nanoparticles (88–100% at pH 7) [59].
731 Emphasize that we observed the maximal yields at the active components
732 concentrations higher by two orders of magnitude that those reported in cited literature.
733 This is an evidence of the participation of a minor part cobalt particles (which are close
734 to the surface) due to steric hindrance for the oxidant to enter the zeolite channels.
735 Hence, the application of fine crystalline zeolites such as ZSM-5 with the large surface
736 area, and mesoporous and hierarchical zeolites ZSM-5 as supports for the water
737 oxidation catalysts seems more promising.

738 An increase in pH of the reaction medium leads expectedly to an increase in the
739 oxygen yield because reaction (IV) of water decomposition is pH-dependent. Inhibiting
740 of the oxygen evolution in the phosphate buffer can be accounted for by the formation
741 of insoluble cobalt phosphates that are catalytically inactive to water oxidation. To
742 check this assumption, we conducted the reaction in the presence of the Co-catalyst at
743 pH 0.8 in the borate and phosphate buffers to reveal that the oxygen yield was no more
744 than 13 % in the phosphate buffer but 56 % in the borate buffer (Fig. 5).

745 The catalyst was tested during five successive cycles under the following
746 conditions: pH 10.0, $[\text{Ru}(\text{bpy})_3^{3+}] = 5 \times 10^{-4}$ M, $[\text{Co}] = 8.13 \times 10^{-4}$ (Fig. 6a). The oxygen
747 yields decreased slightly in every next cycle (64, 63, 61, 60, 60 %) that was caused by
748 the catalyst mechanical losses during its filtering and washing. For example, the catalyst
749 samples weighed initially 120 mg but 102 mg after the fifth cycle. It is important that

750 complex $\text{Ru}(\text{bpy})_3^{2+}$ is strongly sorbed of the surface of 1%Co(6)-ZSM-5(17) that is
751 seen from changes in the catalyst color to light orange, the complex being not washed
752 away with water. To understand the influence of adsorbed $\text{Ru}(\text{bpy})_3^{2+}$ on the catalytic
753 efficiency we tested the same amounts of weighed catalyst samples, both freshly
754 prepared and after reaction with $\text{Ru}(\text{bpy})_3^{3+}$. We conducted two reaction cycles with 120
755 mg of 1%Co(6)-ZSM-5(17) (O_2 yield was 64 %) and merged two portions of the
756 catalyst after filtering and drying. Then we tested once again 120 mg of catalyst with
757 adsorbed Ru-complex collected after the reaction (O_2 yield was 63 %). After washing
758 and drying procedure, the weight of the catalyst decreased to 118 mg; therefore we
759 added the catalyst with adsorbed Ru-complex again to reach 120 mg. We repeated this
760 procedure four times (Fig. 6b) and did not observe any decrease in the O_2 yields. Thus,
761 we can conclude that adsorbed $\text{Ru}(\text{bpy})_3^{2+}$ complexes on the catalyst surface reduces
762 only slightly the O_2 yield only in first cycle that can be accounted for by the competitive
763 adsorption of $\text{Ru}(\text{bpy})_3^{3+}$ (see reaction VII) and $\text{Ru}(\text{bpy})_3^{2+}$ (IX) on the same catalyst
764 sites [Ошибка! Закладка не определена.2]:



766 These facts demonstrate the high stability of the catalysts with respect to the reaction
767 medium and the possibility of its long application for the photocatalytic reaction when
768 the oxidant is generated directly in the reaction medium under the action of light.

769 4. Conclusions

770 Oxo/hydroxo complexes of cobalt (II, III) and nanosize Co_3O_4 particles
771 stabilized in zeolite channels were demonstrated to be effective catalysts for water
772 oxidation by one electron oxidant $\text{Ru}(\text{bpy})_3^{3+}$. The studies of the formation of electron
773 state of cobalt in the zeolite-based catalysts under varied conditions (zeolite structure
774 and silica ratio, procedure for cobalt supporting, cobalt loading, $\text{NH}_4\text{OH}/\text{Co}^{2+}$ ratio,
775 calcination temperature) revealed that polynuclear $\alpha\text{-Co}(\text{OH})_2$ -like clusters and
776 complexes stabilized in zeolite channels are most active to catalytic oxidation of water
777 in the presence of $\text{Ru}(\text{bpy})_3^{2+}$. The transformation of these species to Co_3O_4 -like
778 clusters/nanoparticles and oxocomplexes of Co^{2+} , respectively, during thermal treatment
779 causes some decrease in the catalyst efficiency. The growth of Co_3O_4 -like
780 clusters/nanoparticles in size leads to the further decrease in the system efficiency. The
781 minimal activity is characteristic of the catalysts comprising predominantly isolated
782 $\text{Co}^{2+}_{\text{Oh}}$ ions that indicates a kind of at least polynuclear structure of the catalytically
783 active center Co_nO_x , where $n > 2$.

784 Among the prepared catalysts, 1%Co-ZSM-5(17) prepared by polycondensation
785 at $\text{NH}_4\text{OH}/\text{Co}^{2+}$ ratio equal to 6 was the most effective. In a weak-alkaline medium (pH
786 8.0, 9.2, 10.0) the catalyst provided the yield of oxygen as high as 56, 73 and 78 % of
787 the stoichiometric quantity, respectively. This catalyst was demonstrated in consecutive
788 cycle experiments to be very robust water oxidation catalyst. This makes it promising
789 for photocatalytic oxidation and decomposition of water under the action of light.

790

791 Acknowledgements

792 The work was financially supported by the Russian Science Foundation (Project
793 No. 17-73-300032). This support is gratefully acknowledged.

794 Reference

795 1. Swierk JR, Mallouk TE (2013) Design and development of photoanodes for
796 water-splitting dye-sensitized photoelectrochemical cells. *Chem Soc Rev* 42(6):2357-
797 2387. <https://doi.org/10.1039/c2cs35246j>

798 2. Chikunov AS, Taran OP, Shubin AA, Zil'berberg IL, Parmon VN (2018)
799 Oxidation of Water to Molecular Oxygen by One-Electron Oxidants on Transition
800 Metal Hydroxides. *Kin Catal* 59(1):23–47.
801 <https://doi.org/10.1134/S0023158418010032>.

802 3. Locke E, Jiang S, Beaumont SK (2018) Catalysis of the Oxygen Evolution
803 Reaction by 4–10 nm Cobalt Nanoparticles. *Top Catal* 61(9-11):977-985.
804 <https://doi.org/10.1007/s1124>

805 4. Rosen J, Hutchings GS, Jiao F (2013) Ordered Mesoporous Cobalt Oxide as
806 Highly Efficient Oxygen Evolution Catalyst. *J Am Chem Soc* 135:4516–4521.
807 <https://doi.org/10.1021/ja400555q>

808 5. Chou NH, Ross PN, Bell AT, Tilley TD (2011) Comparison of cobalt-based
809 nanoparticles as electrocatalysts for water oxidation. *ChemCatChem* 4(11):1566-1569.
810 <https://doi.org/10.1002/cssc.201100075>

811 6. Volpato GA, Bonetto A, Marcomini A, Mialane P, Bonchio M, Natali M,
812 Sartorel A (2018) Proton coupled electron transfer from Co_3O_4 nanoparticles to
813 photogenerated $\text{Ru}(\text{bpy})_3^{3+}$: base catalysis and buffer effect. *Sustainable Energy Fuels*.
814 2(9):1951-1956. <https://doi.org/10.1039/c8se00275d>

815 7. Song F, Ding Y, Ma B, Wang C, Wang Q, Du X, Song J. (2013).
816 $\text{K}_7[\text{Co}^{\text{III}}\text{Co}^{\text{II}}(\text{H}_2\text{O})\text{W}_{11}\text{O}_{39}]$: a molecular mixed-valence Keggin polyoxometalate catalyst

817 of high stability and efficiency for visible light-driven water oxidation. *Environ Sci*,
818 6(4):1170. <https://doi.org/10.1039/c3ee24433d>

819 8. Lin J, Meng X, Zheng M, Ma B, Ding Y (2018) Insight into a hexanuclear
820 cobalt complex: strategy to construct efficient catalysts for visible light-driven water
821 oxidation. *Appl Catal B: Environ* 241:351-358. <https://doi.org/10.1016/j.apcatb.2018.09.052>

822 9 Yang C-C, Eggenhuisen TM, Wolters M, Agiral A, Frei H, Jongh PE, Jong
823 KP, Mul G (2013) Effects of Support, Particle Size, and Process Parameters on Co_3O_4
824 Catalyzed H_2O Oxidation Mediated by the $[\text{Ru}(\text{bpy})_3]^{2+}$ Persulfate System.
825 *ChemCatChem* 5(2):550-556. <https://doi.org/10.1002/cctc.201200696>

826 10. Nicholls D (1973) The chemistry of Iron, Cobalt and Nickel. *Comprehensive*
827 *Inorganic Chemistry* 199.

828 11. Song F, More R, Schilling M, Smolentsev G, Azzaroli N, Fox T, Luber S,
829 Patzke GR (2017) $\{\text{Co}_4\text{O}_4\}$ and $\{\text{Co}_x\text{Ni}_{4-x}\text{O}_4\}$ Cubane Water Oxidation Catalysts as
830 Surface Cut-Outs of Cobalt Oxides. *J Am Chem Soc* 139:14198-14208.
831 <https://doi.org/10.1021/jacs.7b07361>

832 12. Pestunova OP, Elizarova GL, Parmon VN (2000) Kinetics and mechanism of
833 water catalytic oxidation by a $\text{Ru}^{3+}(\text{bpy})_3$ complex in the presence of colloidal cobalt
834 hydroxide. *Kin Catal* 41(3):340-348. <https://doi.org/10.1007/BF02755370>

835 13. Deng X, Rin R, Tseng J-C, Weidenthaler C, Apfel U-P, Tüysüz H (2017)
836 Monodispersed Mesoporous Silica Spheres Supported Co_3O_4 as Robust Catalyst for
837 Oxygen Evolution Reaction. *ChemCatChem* 9(22):4238-4243.
838 <https://doi.org/10.1002/cctc.201701001>

839 14. Chen Z, Miao S, Guan J, Zhang F, Li C (2016) Sub-2 nm cobalt oxide
840 cluster catalyst supported on alumina for efficient water oxidation. *Appl Catal A*
841 521:154-159. <https://doi.org/10.1016/j.apcata.2015.11.039>

842 15. Biegun M, Chen X, Mijowska E (2018) Cobalt/Carbon Nanocomposite as
843 Oxygen Evolution Reaction Electrocatalyst. *ChemElectroChem* 5:1-6.
844 <https://doi.org/10.1002/celec.201800355>

845 16. Wang Z, Peng S, Hu Y, Li L, Yan T, Yang G, Ji D, Srinivasan M, Pan Z,
846 Ramakrishna S (2017) Cobalt nanoparticles encapsulated in carbon nanotube-grafted
847 nitrogen and sulfur co-doped multichannel carbon fibers as efficient bifunctional
848 oxygen electrocatalysts. *J Mater Chem A* 5:4949-4961.
849 <https://doi.org/10.1039/C6TA10291C>

- 850 17. Zhang M, Huang Y-L, Wang J-W, Lu T-B (2016) A facile method for the
851 synthesis of a porous cobalt oxide–carbon hybrid as a highly efficient water oxidation
852 catalyst. *J Mater Chem A* 4:1819-1827. [https://doi.org/ 10.1039/C5TA07813J](https://doi.org/10.1039/C5TA07813J)
- 853 18. Meng X, Dong Y, Hu Q, Ding Y (2018) Co Nanoparticles Decorated with
854 Nitrogen Doped Carbon Nanotubes for Boosting Photocatalytic Water Splitting. *ACS*
855 *Sust Chem Engin.* <https://doi.org/10.1021/acssuschemeng.8b05632>
- 856 19. Evangelisti F, Car P-E, Blacque O, Patzke GR (2013) Photocatalytic water
857 oxidation with cobalt-containing tungstobismutates: tuning the metal core. *Catal Sci*
858 *Technol* 3:3117-3129. [https://doi.org/ 10.1039/C3CY00475A](https://doi.org/10.1039/C3CY00475A)
- 859 20. Wei J, Feng Y, Zhou P, Liu Y, Xu J, Xiang R, Ding Y, Zhao C, Fan L, Hu C
860 (2015) A Bioinspired Molecular Polyoxometalate Catalyst with Two Cobalt(II) Oxide
861 Cores for Photocatalytic Water Oxidation. *ChemSusChem* 8(16):2630-4. [https://doi.org/](https://doi.org/10.1002/cssc.201500490)
862 [10.1002/cssc.201500490](https://doi.org/10.1002/cssc.201500490)
- 863 21. Deng X, Tuysuz H (2014) Cobalt-Oxide-Based Materials as Water
864 Oxidation Catalyst: Recent Progress and Challenges, *ACS Catal* 4:3701-3714.
865 [https://doi.org/ 10.1021/cs500713d](https://doi.org/10.1021/cs500713d)
- 866 22. Cejka J, Caorma A, Zones S (2010) Zeolites and Catalysis: Synthesis,
867 Reactions and Applications. *Zeolites and Catalysis: Synthesis, Reactions and*
868 *Applications.* 1-2:881. <https://doi.org/10.1002/9783527630295>
- 869 23. Shrestha S, Dutta PK (2016) Photochemical Water Oxidation by Manganese
870 Oxides Supported on Zeolite Surfaces. *Chem Select* 1:1431–1440. [https://doi.org/](https://doi.org/10.1002/slct.201600208)
871 [10.1002/slct.201600208](https://doi.org/10.1002/slct.201600208)
- 872 24. Krivoruchko OP, Gavrilov VYu, Molina IYu, Larina TV (2008) Distribution
873 of the cobalt-containing component in the pore space of HZSM-5 upon a postsynthetic
874 modification of the zeolite with hydroxo compounds of Co^{2+} . *Kin Catal* 49(2):285-
875 290. <https://doi.org/10.1134/S0023158408020171>
- 876 25. Yashnik SA, Salnikov AV, Vasenin NT, Anufrienko VF, Ismagilov ZR
877 (2012) Regulation of the copper-oxide cluster structure and DeNO_x activity of Cu-ZSM-
878 5 catalysts by variation of OH/Cu^{2+} . *Catal Tod* 197:214-227.
879 <https://doi.org/10.1016/j.cattod.2012.08.033>
- 880 26. Creuts C, Sutin N (1975) Reaction of $\text{Ru}(\text{bpy})_3^{3+}$ with hydroxide and its
881 application in a solar energy storage system. *Proc Nat Acad Sci USA* 72:2855-2862.
- 882 27. Anastas PT, Warner JC (1998) *Green Chemistry: Theory and Practice.* – N.-
883 Y.: Oxford University Press. 30.

- 884 28. Yashnik SA, Ismagilov ZR, Anufrienko VF (2005) Catalytic Properties and
885 Electronic Structure of Copper Ions in Cu-ZSM-5. *Cat Tod* 110:310-322.
886 <https://doi.org/10.1016/j.cattod.2005.09.029>
- 887 29. Tomic-Tucakovic B, Majstorovic D, Jelic D, Mentus S (2012)
888 Thermogravimetric study of the kinetics of Co_3O_4 reduction by hydrogen.
889 *Thermochimica Acta* 541:15–24. <https://doi.org/10.1016/j.tca.2012.04.018>
- 890 30. Lever ABP (1984) *Inorganic Electron Spectroscopy*, Elsevier, Vol. 2.
- 891 31. Dedecek J, Kaucky D, Wichterlova B (2000) Co^{2+} ion siting in pentasil-
892 containing zeolites, part 3. Co^{2+} ion sites and their occupation in ZSM-5: a VIS diffuse
893 reflectance spectroscopy study. *Microporous and Mesoporous Materials* 35–36:483–
894 494. [https://doi.org/10.1016/S1387-1811\(99\)00244-9](https://doi.org/10.1016/S1387-1811(99)00244-9)
- 895 32. Dedecek J, Capek L, Kaucky D, Sobalik Z, Wichterlova B (2002) Siting and
896 distribution of the Co ions in beta zeolite: a UV–Vis–NIR and FTIR study. *J Catal*
897 211:198–207. <https://doi.org/10.1006/jcat.2002.3697>
- 898 33. Cruz RS, Mascarenhas AJS, Andrade HMC (1998) Co-ZSM-5 catalysts for
899 N_2O decomposition. *Appl Catal B* 18:223–231. [https://doi.org/10.1016/S0926-](https://doi.org/10.1016/S0926-3373(98)00042-3)
900 [3373\(98\)00042-3](https://doi.org/10.1016/S0926-3373(98)00042-3)
- 901 34. El-Malki E-M, Werst D, Doan PE, Sachtler WMH (2000) Coordination of
902 Co^{2+} Cations inside Cavities of Zeolite MFI with Lattice Oxygen and Adsorbed
903 Ligands. *J Phys Chem B* 104:5924-5931. <https://doi.org/10.1021/jp000540i>
- 904 35. Gil B, Pietrzyk P, Datka J, Kozyra P, Sojka Z (2005) Speciation of cobalt in
905 CoZSM-5 upon thermal treatment. *Stud Surf Sci Catal* 158:893–900.
906 [https://doi.org/10.1016/S0167-2991\(05\)80427-6](https://doi.org/10.1016/S0167-2991(05)80427-6)
- 907 36. Baes CFJr, Mesmer RE (1976) *The Hydrolysis of cations*. New York: Wiley,
908 Interscience, 267-274.
- 909 37. Jayashree RS, Vishnu Kamath P (1999) Electrochemical synthesis of a-
910 cobalt hydroxide. *J Mater Chem* 9:961–963. <https://doi.org/10.1039/A807000H>
- 911 38. Krivoruchko OP, Larina TV, Anufrienko VF, Molina IYu, Paukshtis EA
912 (2009) Synthesis, Electronic State, and Particle Size Stabilization of Nanoparticulate
913 $[\text{Co}(\text{OH})_2(\text{H}_3\text{O})^{\text{d}+}]^{\text{d}+}$. *Inorg Matt* 45(12):1355-1361.
914 <https://doi.org/10.1134/S0020168509120097>
- 915 39. Liu PF, Yang S, Zheng LR, Zhang B, Yang HG (2016) Electrochemical
916 etching of a-cobalt hydroxide for improvement of oxygen evolution reaction. *J Mater*
917 *Chem A* 4:9578–9584. <https://doi.org/10.1039/C6TA04078K>

918 40. Zhao Z, Geng F, Bai J, Cheng H_M (2007) Facile and Controlled Synthesis
919 of 3D Nanorods-Based Urchinlike and Nanosheets-Based Flowerlike Cobalt Basic Salt
920 Nanostructures. *J Phys Chem C* 111:3848-3852. [https://doi.org/ 10.1021/jp067320a](https://doi.org/10.1021/jp067320a)
921 41. Chapman B (2004) *Transition Metals, Quantitative Kinetics and Applied*
922 *Organic Chemistry*. Nelson Thornes Ltd. 142.
923 42. Jeevanandam P, Kolytyn Yu, Gedanken A, Mastai Y (2000) Synthesis of a-
924 cobalt(II) hydroxide using ultrasound radiation. *J Mater Chem* 10:511-514.
925 [https://doi.org/ 10.1039/A908065A](https://doi.org/10.1039/A908065A)
926 43. Brownson JRS, Levy-Clement C (2009) Nanostructure α - and β -cobalt
927 hydroxide thin films. *Electrochimica Acta* 54:6637-6644
928 44. Wang X, Chen H, Sachtler WMH (2001) Selective reduction of NO_x with
929 hydrocarbons over Co/MFI prepared by sublimation of CoBr₂ and other methods. *Appl*
930 *Catal B* 29:47-60. [https://doi.org/ 10.1016/S0926-3373\(00\)00186-7](https://doi.org/10.1016/S0926-3373(00)00186-7)
931 45. Bustamante F, Cordoba F, Yates M, Montes de Correa C (2002) The
932 promotion of cobalt mordenite by palladium for the lean CH₄-SCR of NO_x in moist
933 streams. *Appl Catal A: Gen* 234:127-136. [https://doi.org/10.1016/S0926-](https://doi.org/10.1016/S0926-860X(02)00211-9)
934 [860X\(02\)00211-9](https://doi.org/10.1016/S0926-860X(02)00211-9)
935 46. Resini C, Montanari T, Nappi L, Bagnasco G, Turco M, Busca G, Bregani F,
936 Notaro M, Rocchini G (2003) Selective catalytic reduction of NO_x by methane over Co-
937 H-MFI and Co-H-FER zeolite catalysts: characterisation and catalytic activity. *J Catal*
938 214:179 - 190. [https://doi.org/10.1016/S0021-9517\(02\)00153-7](https://doi.org/10.1016/S0021-9517(02)00153-7)
939 47. Bagnasco G, Turco M, Resini C, Montanari T, Bevilacqua M, Busca G
940 (2004) On the role of external Co sites in NO oxidation and reduction by methane over
941 Co-H-MFI catalysts. *J Catal* 225:536-540. . <https://doi.org/10.1016/j.jcat.2004.04.011>
942 48. Ulla MA, Gutierrez L, Lombardo EA, Lonyi F, Valyon J (2004) Catalytic
943 features of Pt,Co-mordenite for the SCR of NO_x monitored by DRIFT spectroscopy
944 using adsorbed N₂ as a probe. *Appl Catal A: Gen* 277:227-237.
945 <https://doi.org/10.1016/j.apcata.2004.09.016>
946 49. Bellmann A, Atia H, Bentrup U, Bruckne A (2018) Mechanism of the
947 selective reduction of NO_x by methane over Co-ZSM-5. *Appl Catal B* 230:184-193.
948 <https://doi.org/10.1016/j.apcatb.2018.02.051>
949 50. Yashnik SA, Ismagilov ZR (2015) Cu-substituted ZSM-5 catalyst:
950 controlling of DeNO_x reactivity via ion-exchange mode with copper-ammonia solution.
951 *Appl Catal B* 170-171:241-254. <https://doi.org/10.1016/j.apcatb.2015.01.021>

- 952 | 51. Sivan V, Iyengar GNK (1976) Reduction kinetics of cobaltic oxide (Co_3O_4)
953 | in hydrogen, *Trans. Indian Inst. Met.* 29:83–91;
- 954 | 52. Sexton BA, Hughes AE, Turney TW (1986) An XPS and TPR Study of the
955 | Reduction of Promoted Cobalt-Kieselguhr Fischer-Tropsch Catalysts. *J Catal* 97:390-
956 | 406. [https://doi.org/10.1016/0021-9517\(86\)90011-4](https://doi.org/10.1016/0021-9517(86)90011-4)
- 957 | 53. Wu R-J, Wu J-G, Tsai T-K, Yeh C-T (2006) Use of cobalt oxide CoOOH in
958 | a carbon monoxide sensor operating at low temperatures. *Sensors and Actuators B*
959 | 120:104–109
- 960 | 54. Rosynek MP, Polansky ChA (1991) Effect of cobalt source on the reduction
961 | properties of silica-supported cobalt catalysts. *App Catal* 73:97-112.
962 | [https://doi.org/10.1016/0166-9834\(91\)85115-C](https://doi.org/10.1016/0166-9834(91)85115-C)
- 963 | 55. Xie R, Li D, Hou B, Wang J, Jia L, Sun Y (2011) Silylated Co_3O_4 -m- SiO_2
964 | catalysts for Fischer–Tropsch synthesis. *Catalysis Communications* 12:589–592.
965 | <https://doi.org/10.1016/j.catcom.2010.12.013>
- 966 | 56. Tang C-W, Wang C-B, Chien S-H (2008) Characterization of cobalt oxides
967 | studied by FT-IR, Raman, TPR and TG-MS. *Thermochimica Acta* 473:68–73.
968 | <https://doi.org/10.1016/j.tca.2008.04.015>
- 969 | 57. Suga M, Akita F, Sugahara M, Kubo M, Nakajima Y, Nakane T, Yamashita
970 | K, Umena Y, Nakabayashi M, Yamane T, Nakano T, Suzuki M, Masuda T, Inoue S,
971 | Kimura T, Nomura T, Yonekura S, Yu LJ, Sakamoto T, Motomura T, Chen JH, Kato Y,
972 | Noguchi T, Tono K, Joti Y, Kameshima T, Hatsui T, Nango E, Tanaka R, Naitow H,
973 | Matsuura Y, Yamashita A, Yamamoto M, Nureki O, Yabashi M, Ishikawa T, Iwata S,
974 | Shen JR (2017) Light-induced structural changes and the site of O=O bond formation in
975 | PSII caught by XFEL. *Nature* 543(7643):131-135. <https://doi.org/10.1038/nature21400>
- 976 | 58. Akhtar US, Tae EL, Chun YS, Hwang IC, Yoon KB (2016) Insights into
977 | decomposition pathways and fate of $\text{Ru}(\text{bpy})_3^{2+}$ during photocatalytic water oxidation
978 | with $\text{S}_2\text{O}_8^{2-}$ as sacrificial electron acceptor. *ACS Catal* 6(12):8361-8369. <https://doi.org/10.1021/acscatal.6b02595>
- 980 | 59. Barelocher C, McCusker LB, Olson DH (2007) Atlas of Zeolite Framework
981 | Types. 6th Revised Edition. Eds.: Elsevier, Amsterdam.
- 982 | 60. Biner M, Buergi HB, Ludi A, Roehr C (1992) Crystal and molecular
983 | structures of $[\text{Ru}(\text{bpy})_3](\text{PF}_6)_3$ and $[\text{Ru}(\text{bpy})_3](\text{PF}_6)_2$ at 105 K. *J Am Chem Soc*
984 | 114(13):5197–5203. <https://doi.org/10.1021/ja00039a034>

- 985 61. Zidki T, Zhang L, Shafirovich V, Lyman SV (2012) Water Oxidation
986 Catalyzed by Cobalt(II) Adsorbed on Silica Nanoparticles. *J Am Chem Soc* 134:14275–
987 14278. <https://doi.org/10.1021/ja304030y>.
- 988 62. Bainbridge M, Clarkson JS, Parnham BL, Tabatabaei J, Tyers DV, Waugh
989 KC (2017) Evidence for support effects in metal oxide supported cobalt catalysts. *Cat*
990 *Struct React* 3(3):128-137, <https://doi.org/10.1080/2055074X.2017.1281718>
- 991 63. Park K-W, Kolpak AM (2018) Understanding photocatalytic overall water
992 splitting on CoO nanoparticles: Effects of facets, surface stoichiometry, and the
993 CoO/water interface. *J Catal* 365:115–124. <https://doi.org/10.1016/j.jcat.2018.06.021>
- 994 64. Porkrant S, Dilger S, Landsmann S, Trottmann M (2017) Size effects of
995 cocatalysts in photoelectrochemical and photocatalytic water splitting. *Mat Tod Energ*
996 158-163. <https://doi.org/10.1016/j.mtener.2017.06.005>
- 997 65. Chikunov AS, Taran OP, Pyshnaya IA, Parmon VN (2019) Colloidal Fe^{III},
998 Mn^{III}, Co^{III}, and Cu^{II} Hydroxides Stabilized by Starch as Catalysts of Water Oxidation
999 Reaction with One Electron Oxidant Ru(bpy)₃³⁺. *ChemPhysChem* 20:410-421.
1000 <https://doi.org/10.1002/cphc.201800957>
- 1001 66. Yin Q, Tan JM, Besson C, Geletii YV, Musaev DG, Kuznetsov AE, Luo Z,
1002 Hardcastle KI, Hill CL (2010) A Fast Soluble Carbon-Free Molecular Water Oxidation
1003 Catalyst Based on Abundant Metals. *Science* 328:342-345.
1004 <https://doi.org/10.1126/science.1185372>